Journal of *Marine Science and Engineering*

MDPI

Article

Numerical Simulation Investigation of Vortex Finder Depth Effects on Flow Field and Performance of Desanding Mini-Hydrocyclones

Fengqin He [1,*], Decao Zhao [1], Jiangang Wang [2], Yuan Huang [3] and Qibin Liu [1]

[1] The College of Information, Mechanical and Electrical Engineering, Shanghai Normal University, Shanghai 200234, China
[2] College of Mechanical Engineering, Shanghai Institute of Technology, Shanghai 201418, China
[3] Institute of Environmental Pollution and Health, School of Environmental and Chemical Engineering, Shanghai University, Shanghai 200444, China
* Correspondence: hfq@shnu.edu.cn

Abstract: Sand has significant side effects on oil production and offshore platform processing system. Mini-hydrocyclones is a very important component to desanding operation system. However, even a slight modification on the structural parameter of hydrocylone might result in a significant influence on its flow field and separation efficiency. So, analysis on flow field characteristics and separation efficiency of the mini-hydrocyclones can help to optimize its structural parameters. In this work, five mini-hydrocycloness were designed, and flow patterns and particle separation ability of a mini-hydrocyclones with various vortex finder depths were investigated through Computational Fluid Dynamics (CFD) simulation method. The research shows that vortex finder depth has a significant influence on the separation function partition of mini-hydrocyclones. The deeper the vortex finder depth is, the larger the volume of pre-separation area, the smaller the volume of the main separation area and the bigger the energy consumption are. These characteristics are disadvantage to improve separation performance of hydrocyclone. Ratio (L_0/D) of vortex finder depth (L_0) to the hydrocyclone cylinder diameter (D) is about 1.0.

Keywords: mini-hydrocyclones; vortex finder; computational fluid dynamic; separation efficiency; desanding

Citation: He, F.; Zhao, D.; Wang, J.; Huang, Y.; Liu, Q. Numerical Simulation Investigation of Vortex Finder Depth Effects on Flow Field and Performance of Desanding Mini-Hydrocyclones. *J. Mar. Sci. Eng.* **2022**, *10*, 1600. https://doi.org/10.3390/jmse10111600

Academic Editor: María Isabel Lamas Galdo

Received: 30 September 2022
Accepted: 26 October 2022
Published: 31 October 2022

1. Introduction

The probability of prospecting onshore integrated oil fields is gradually dropping, and offshore oil is becoming an essential source of crude oil production. The produced fluid from offshore oil wells contains a large amount of produced water, sediment and other mechanical impurities. After preliminary separating operation by the treatment facility, the three-phases of oil, gas, water and the large solid particles can be separated. Because the feed components are very complicated, the requirements of operation flexibility, adaptability and anti-fluctuation of the pretreatment device are quite strict, whereas the separation efficiency of the device is not strictly pursued. So, the oil-water mixture produced from preliminary equipment still carries a large amount of fine mud and sand particles. It is easy to lead pipeline blockage and flow passage components abrasion [1–3]. In order to improve the quality of crude oil and better equipment maintenance, it is necessary to further remove these fine solid particles. Hydrocyclone is a common device used in minerals [4,5], pharmaceuticals [6,7], petrochemicals [8,9] and sewage treatment industries [10,11] because of its low operating cost, easy maintenance, high throughput, etc . . . Moreover, numerous studies on hydrocyclone [10–12] indicated that fine particle sizes (5–20 μm) are difficult to remove by conventional hydrocyclone, but mini-hydrocycloness can effectively remove micron-size particles larger than 3 microns because the cut sizes of hydrocyclone

are directly proportional to its diameter. A mini-hydrocyclones (Figure 1) has identical cylindrical geometry and configuration similar to a conventional hydrocyclone. Nowadays, mini-hydrocycloness are widely used in wastewater, produced fluid from offshore oil wells treatment, even used in separate mammalian cells [12]. However, the performance of mini-hydrocycloness is highly dependent on their geometrical characteristics such as cylindrical section diameter, core angle, vortex finder depth, feed inlet geometry, and so on. Thus, during the development of a novel hydrocyclone, lots of experiments need be conducted to optimize parameters of hydrocyclone and verify its effects. Many investigations [13–17] concluded that the annular gap between the cylindrical wall and vortex finder plays the role of preliminary separation function in hydrocyclones.

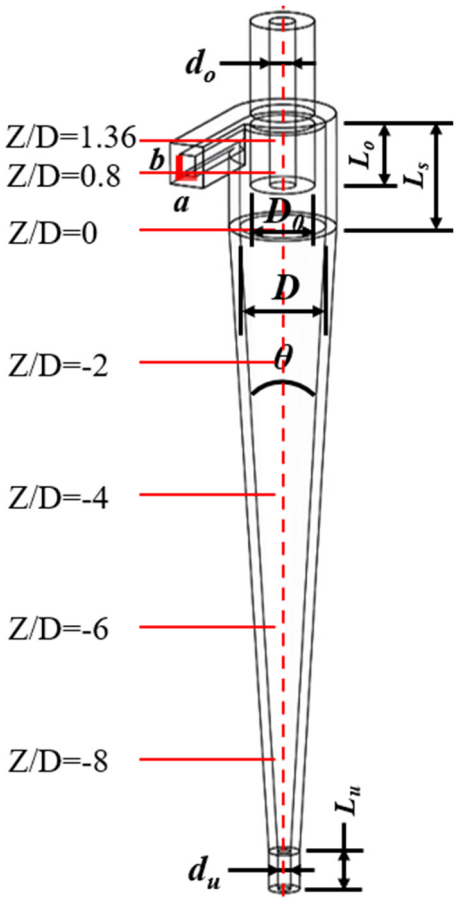

Figure 1. Structure figure of mini-hydrocyclone.

As an indispensable unit of hydrocyclone, vortex finder geometry is the critical parameters. It affects the structure of preliminary separation space and the split ratio. Optimizing the structural parameters of the vortex finder not only can reduce the phenomenon which the coarse particles escape from vortex finder directly, but also optimize performance of hydrocyclone. In the past decades, some scholars [13–17] have investigated the effects of different diameter or shape of the vortex finder. Nevertheless, the vortex finder depth investigation using numerical simulation is seldom involved in the published analyses. Actually, it has a significant influence on short-circuit flow, circulation flow, and the main separation space [12,13,15]. Wang et al. [16] investigated the flow field of hydrocyclone with different configuration of vortex finder by CFD method. Zhao et al. [18] concluded that thin-walled vortex finder helps improve separation sharpness. Oliveira et al. [19] reported that a higher insertion depth of the vortex finder provides a higher resistance to the fluid flow in the hydrocyclone. Although the research conclusions are not uniform, the consensus [12,13,20] is that the end of the vortex finder should not locate in cone segment.

Mini-hydrocycloness are more suitable for separating fine particles than conventional hydrocyclones, which has been confirmed by lots of investigations [21–24]. However, as is well known, exploring a novel hydrocyclone via experiment is a time-consuming and expensive operation. Computational fluid dynamics (CFD) is an effective tool to understand multiphase flow, which has been proved, and successfully used to explore novel hydrocyclone [25–33]. The objective of this study is to find out the optimal vortex finder depth.

2. Numerical Modeling and Solution Method

2.1. Physical Model and Discrete Grids

In order to investigate the influence of vortex finder depth on the flow filed and separation performance of mini-hydrocycloness, five mini-hydrocycloness were designed; they share nearly identical structural parameters except for different vortex finder depths. The schematic diagram and dimensions of mini-hydrocycloness used in the present study are showed in Figure 1 and Table 1. In order to ensure the accuracy of the calculation and the high-quality mesh, the method which it generates grids by partition was adopted. The whole mini-hydrocyclones model is divided into six parts: the inlet section is divided into two sections, the ring gap formed between the vortex finder and the cylinder wall is cut into two zones, the remaining zones of the cylinder and the cone are combined into one zone, and the vortex finder is as one zone. Except the vortex finder partition area used the cooper grids, the other zones mesh in hexahedral structured grid. The meshed mini-hydrocyclones model is shown in Figure 2. The five mini-hydrocycloness have the same grid structures except for the difference vortex finder depth. The grids of different mini-hydrocycloness are 600,000~700,000. The worst grid quality values are 0.71643 or so.

Table 1. Mini-hydrocyclones structure parameters in the fluent simulation.

Mini-hydrocyclones	No.1	No.2	No.3	No.4	No.5
L_0/D	0.8	1.0	1.2	1.32	1.4
L_0/L_s	0.57	0.71	0.86	0.94	1
$a \times b$ (mm × mm)	4 × 8	4 × 8	4 × 8	4 × 8	4 × 8
d_u/D	0.12	0.12	0.12	0.12	0.12
d_0/D	0.28	0.28	0.28	0.28	0.28
$\theta(^\circ)$	6	6	6	6	6
D_0/D	0.68	0.68	0.68	0.68	0.68

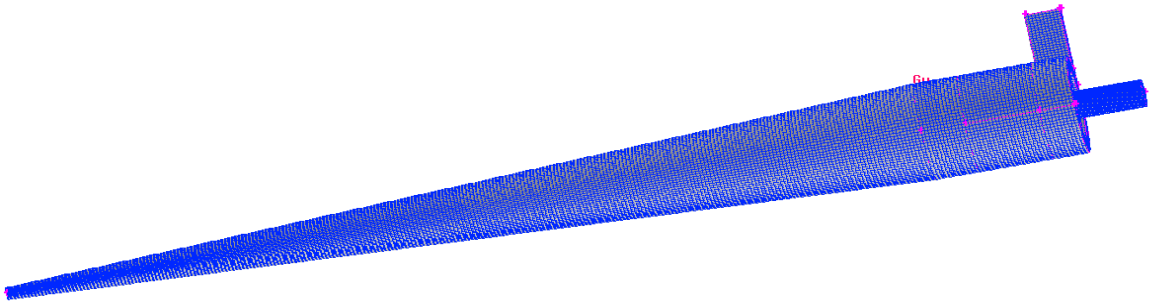

Figure 2. Grids of mini-hydrocyclones computational domain.

2.2. Mathematics Model

The most widely used turbulent mathematical models in numerical continuous phase simulation method for hydrocyclone separation process are k-ε, k-ε RNG, large eddy simulation (LES), direct numerical simulation (DNS), Reynolds stress model (RSM) and so on. Due to the anisotropy of the turbulent in the strong cyclone flow field of hydrocyclone, the k-ε model cannot accurately describe the flow field in hydrocyclone. LES is a kind of spatial average of turbulence pulsation, and it cannot be widely used in engineering

because of the high computational cost [34,35]. DNS does not need to model the turbulence, and control equation is directly solved by numerical calculation. In order to obtain the flow information of all scales, the DNS computation is large, time-consuming, and the dependence on computer memory is strong. RSM along with unsteady Reynolds averaged Navier–Stokes (RANS) formulation has proven to be an appropriate turbulence model for cyclone flow [23,24,26–30]. Its computing costs are also less expensive than LES and DNS.

Equations (1) and (2) are continuous equations and momentum equations for RMS model, respectively. Equation (3) is the Reynolds stress transport equation. Equations (4)–(9) are diffusion item, shear force generation item, pressure strain item and turbulent energy consumption item, respectively. Equations (1)–(9) constitute the closed equations of The RSM model.

$$\frac{\partial(\rho U_j)}{\partial x_j} = 0 \tag{1}$$

$$\frac{\partial(\rho U_i U_j)}{\partial x_j} = -\frac{\partial p}{\partial x_i} + \frac{\partial}{\partial x_j}\left(\mu\left(\frac{\partial U_i}{\partial x_j} + \frac{\partial U_j}{\partial x_i}\right) - \rho\overline{u_i{}'u_j{}'}\right) \tag{2}$$

$$\frac{\partial}{\partial t}\left(\rho\overline{u_i{}'u_j{}'}\right) + \frac{\partial}{\partial x_k}\left(\rho U\overline{u_i{}'u_j{}'}\right) = D_{ij} + p_{ij} + \prod_{ij} + \varepsilon_{ij} \tag{3}$$

$$D_{ij} = -C_\mu\rho\frac{k}{\varepsilon}u_k{}'u_l{}'\frac{\partial}{\partial x_k}\left(u_i{}'u_j{}'\right) \tag{4}$$

$$p_{ij} = -\rho\left[\overline{u_i{}'u_k{}'}\frac{\partial U_j}{\partial x_k} + \overline{u_j{}'u_k{}'}\frac{\partial U_i}{\partial x_k}\right] \tag{5}$$

$$\prod_{ij} = \prod_{ij1} + \prod_{ij2} \tag{6}$$

$$\prod_{ij1} = -C_1\rho\frac{\varepsilon}{k}\left(\overline{u_i{}'u_k{}'} - \frac{2}{3}\delta_{ij}k\right) \tag{7}$$

$$\prod_{ij2} = -C_2\left(P_{ij} - \frac{2}{3}\delta_{ij}G_k\right) \tag{8}$$

$$\varepsilon_{ij} = \frac{2}{3}\delta_{ij}\rho\varepsilon \tag{9}$$

2.3. Numerical Setting

To numerical setting of continuous phase simulation, the initial calculation of the turbulence intensity I, the turbulent kinetic energy k, and the turbulent dissipation rate ε can be calculated by Equations (10)–(12). 'VELOCITY INLET' was chosen as the boundary condition of the inlet, and parameters of inlet boundary are shown in Table 2. The outlet boundary condition adopts 'OUTFLOW' which was current widely used. The split ratio of mini-hydrocyclones was set to 10%. Wall surface uses 'NON-SLIP BOUNDARY', assuming that the walls are smooth surfaces. Pressure-velocity coupling choose 'SIMPLEC' algorithm, 'GREEN-GAUSS CELL BASED' is regarded as the gradient spatial discretization, 'PRESTO' is set as the pressure spatial discretization, and momentum, turbulent kinetic energy, and turbulent dissipation rate use 'SECOND ORDER UPWIND'.

Table 2. Boundary parameters of the inlet.

Parameters	Value	Unit
Inlet velocity (u_{in})	7.6	m/s
Reynolds number (Re_{D_H})	3.244×10^4	
Turbulence intensity (I)	4.25	%
Dydraulic diameter (D_H)	5.3	mm
Turbulent kinetic energy (k)	0.6812	m^2/s^2
Turbulent dissipation rate (ε)	33.1492	m^2/s^3

The disperse phase is simulation based on the preliminary flow field from the continuous phase simulation. 'SAFFMAN LIFT FORCE' and 'PRESSURE GRADIENT FORCE' were selected into the physical models. Accuracy control to the numerical method was set at 1×10^{-5}. The particles spray in the direction of the normal line of the surface, and the particles inlet velocity is consistent with the continuous phase simulation. The drag force criterion is spherical, and particles rotation is enabled. The rotation drag force criterion is 'DENNIS-EL-AL'. Magnus lift law chose 'OESTERLE-BUI-DINH'. The solution method is the same as continuous phase. The dispersed phase simulation time is set to transient format, and the particle migration motion adopts the dispersed phase model (DPM). The boundary conditions of discrete phase are set as follows: BC type of the underflow section is 'TRAP' and vortex finder outlet is 'ESCAPE'. The dispersed phase adopts inertial particles with a density of 2100 kg/m^3. The mass flow rate of particle in the present study is set as 0.0001 kg/s. The simulation process of dispersed phase is as follows: 1. opening DPM model; 2. creating particle injection; 3. turning on reports of discrete phase sample; 4. running calculation; 5. closing the sampling process after the residual reaches stability. The separation efficiency is calculated as Equation (13)

$$I = u'/\overline{u} = 0.16\left(\mathrm{Re}_{D_H}\right)^{-1/8} \tag{10}$$

$$k = \frac{3}{2}(\overline{u}I)^2 \tag{11}$$

$$\varepsilon = C_\mu^{3/4}\frac{k^{3/2}}{l} \tag{12}$$

$$\eta = \frac{m_u}{m} \tag{13}$$

3. Experimental Validation and Analysis

3.1. Continuous Phase Simulation Validation

The validation of the present flow field simulation was performed by a comparison between the obtained numerical results and the measured flow field from the literature as He et al. [12]. The flow field was measured by Particle Image Velocimetry (PIV) technique. The mini-hydrocyclones structure parameters are set as the same in PIV experiment and the CFD calculation, vortex finder depth is 25 mm. PIV experiment operation condition is 875 L/h, the corresponding CFD simulation inlet velocity is 7.6 m/s. Figure 3 is the comparison result of local axial velocity in half plane of the interface cross-section between the cone and the column. The deviation is 10% or so when the radius coordination between 5 mm to 12.5 mm. It becomes bigger as the location gets closer to the air cone. This is because the radial movement of air bubble has influence on the axial velocity in the PIV experiment. Experiment also can be affected by wave of operation condition and material condition, and CFD simulation calculation environments are more ideal. It can also be seen in Figure 3 that the trend of axial velocity is identical. It proves that the present model and method are valid and meaningful for further field flow simulations.

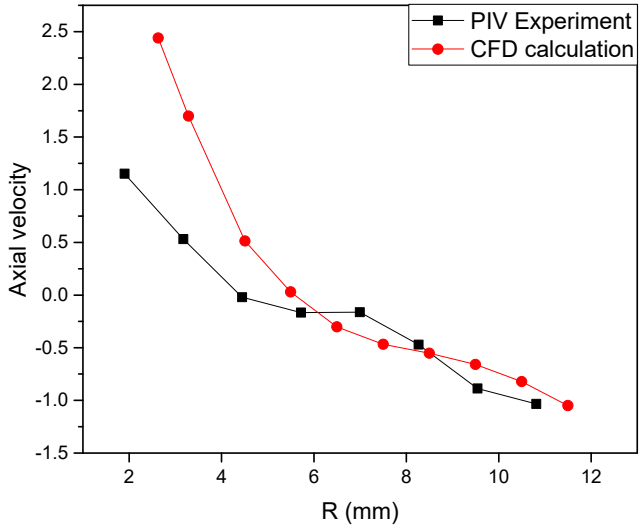

Figure 3. Axial velocity compared between experiment and calculation.

3.2. Dispersed Phase Simulation Verification

In order to verify the CFD simulation accuracy of the discrete phase, it is necessary to compare the simulation results of the dispersed phase with the actual separation efficiency of hydrocyclone. Figure 4 is the separation experimental equipment. Fluid Catalytic Cracking (FCC) catalyst and water were fully mixed in the feed tank and mixture concentration is 400 mg/L. the mixture is pumped into the pipeline by a centrifugal pump. The bumper tank in the equipment is set in order to reduce the fluid fluctuation. A return line was set between the outlet of the centrifugal pump and feed tank to manipulate the feed rate. The most light-phase returned to the feed tank from the vortex finder, whereas the most heavy-phase returned the feed tank from the underflow orifice. The flow meters and pressure gauges were set on the pipeline of inlet of mini-hydrocylone. The gauges were also set on the pipeline of the overflow and underflow pipelines. Sampling process should begin after experiment setup running for some minutes and reaching a stable working condition. The samples should be filtered, dried, and weighed. Then, the mass flow rate of solid particles at the inlet and underflow can be obtained. The separation efficiency of mini-hydrocyclone is the ratio of the mass flow rate of particles from the underflow outlet to the solid particle mass flow rate at the feed inlet.

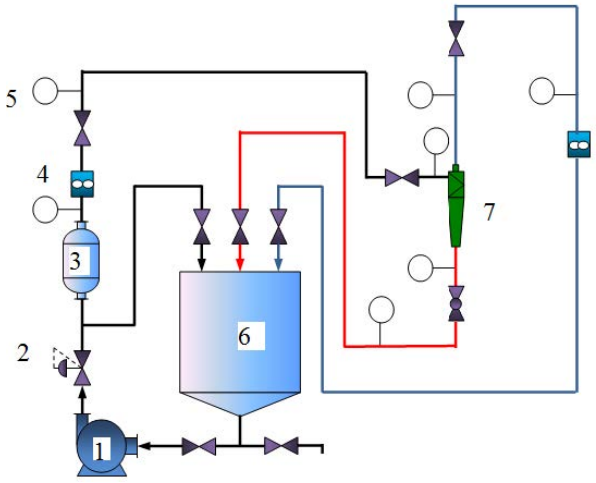

Figure 4. Separation procedure of experimental equipment. 1. centrifugal pump 2. equalizer valve 3. bumper tank 4. flow meter 5. gauge meter 6. feed tank 7. hydrocyclone.

Comparison chart of separation efficiency between simulation and experiment is shown in Figure 5, and they are separation efficiencies of No.1 mini-hydrocyclone in Table 1 with different inlet flow velocity. It can be seen that the variation trend is basically consistent between the simulated separation efficiency and experimental separation efficiency under different inlet flow rates. Simulation data is 1–3% higher than experiment data under most operating conditions, and the reason is the same as the deviation in Figure 3. Comparative analysis of separation efficiency data reveals feasibility of CFD discrete phase simulation method.

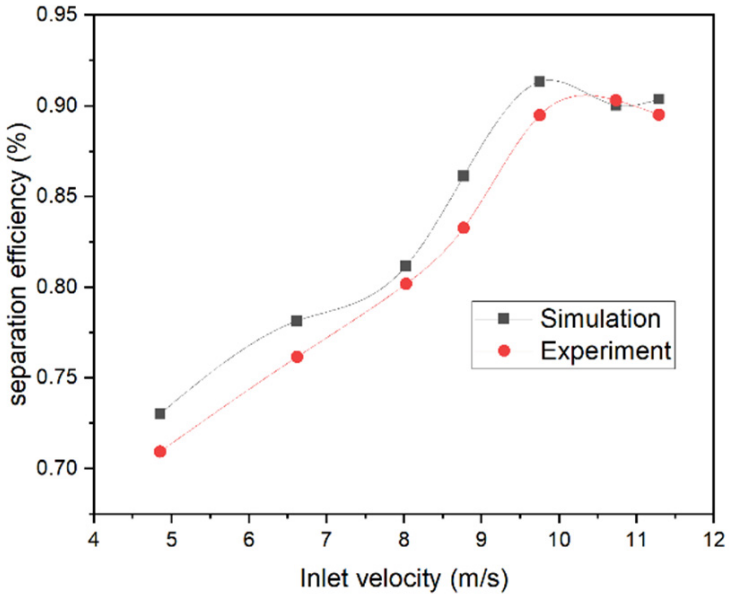

Figure 5. Comparison chart of separation efficiency between simulation and experiment.

4. Results and Discussion

4.1. Continuous Phase

Cloud maps with flow field information and velocity of continuous phase on seven Z-axial positions of mini-hydrocyclones can be extracted from the CFD simulation file. The seven Z-axial positions are shown in Figure 1. The flow field information can be qualitatively analyzed using cloud maps; it also can be quantitatively analyzed by the velocity data.

4.1.1. Analysis of Radial Velocity Simulation

It can be observed from the radial velocity cloud diagram in Figure 6 that the radial velocity is much smaller than axial and tangential velocities. The deeper the vortex finder inserts, the smaller the radial velocity is. Radial velocity determines the radial migration activity of particles, which directly affects separation efficiency. On both sides of the central axis of mini-hydrocyclones, the radial velocity is opposite in direction, but amplitude is close. Radial velocity distribution of the mini-hydrocyclones with L_0/D of 0.8 and 1.0 is more regular than the other three mini-hydrocycloness. The mini-hydrocyclones with L_0/D of 1.0 has the biggest radial velocity in the main separation zone.

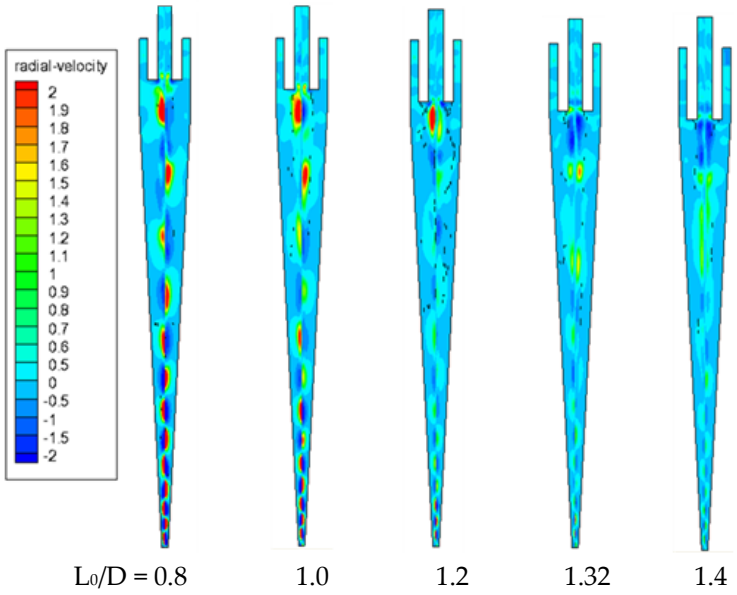

Figure 6. Radial velocity cloud figure of mini-hydrocycloness with different vortex finder depth.

4.1.2. Axial Velocity Simulation Results

It can be found in Figure 7 that circulating flow exists in the ring gap between the vortex finder and the cylinder section wall. In the cone section, the axial velocity of the upward flow reaches a maximum at a 2 mm circumference radius, and the maximum axial velocity of the downward flow is located in the region of 1.7–2 mm away from the wall of mini-hydrocyclones. In the middle and lower part of the cone section, the axial velocity of downward flow increases first and then decrease gradually till the LZVV from the wall to the center of the mini-hydrocyclones. Similarly, upward flow axial velocity increases first and then decrease until it changes to downward flow. This phenomenon proves that, except the particle in the external swirl flow, some particles in the internal swirl flow have chance to be separated again in the middle and lower part of mini-hydrocyclones.

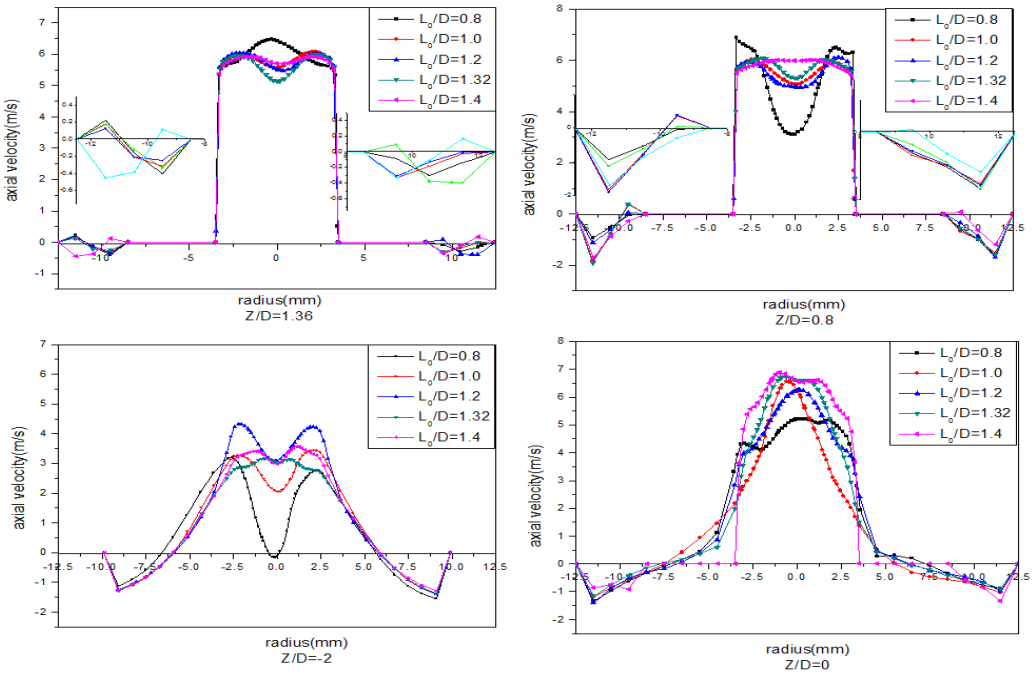

Figure 7. *Cont.*

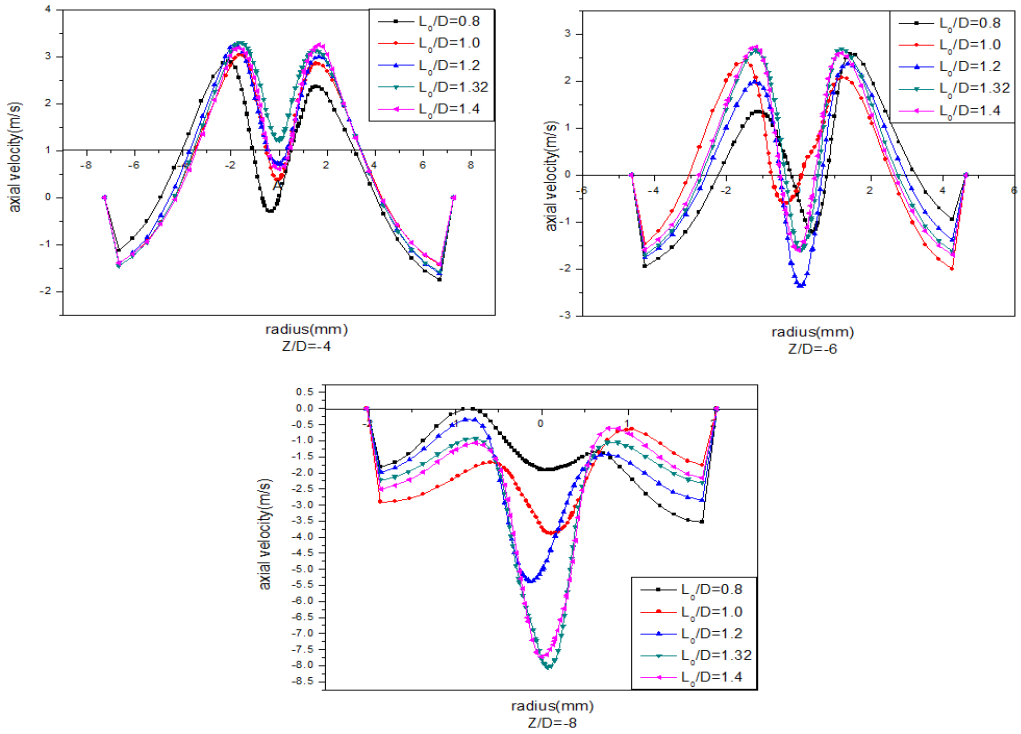

Figure 7. Comparative analysis chart of the axial velocity of mini-hydrocycloness.

4.1.3. Analysis of Tangential Velocity Simulation

It illustrates in Figure 8 that, from the wall to the central axis, tangential velocity gradually increases, reaching the maximum near the air column. At the position of the junction interface (the cross-section Z = 0) of the cylinder and cone, the tangential velocity shows a concave phenomenon in the quasi-free region, which is the result of vortex finder affecting the flow field. It indicates that there exists a tangential velocity gradient zone. Particles stay in this area for more time than other regions. Thus, forming highly concentrated zone of dispersed phase. It seriously affects the separation efficiency of the mini-hydrocyclones. The deeper the vortex finder depth is, the more easily the particles are aggregated. Tangential velocity curve is the least concave in the mini-hydrocyclones with L_0/D of 1.0.

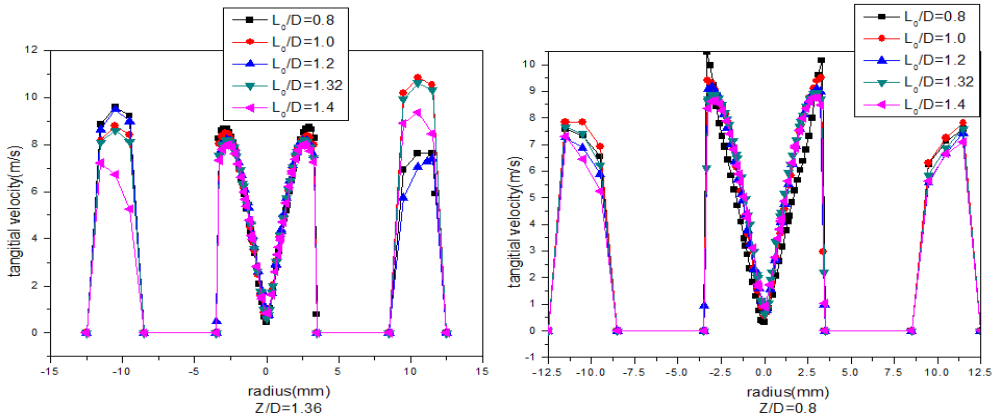

Figure 8. *Cont.*

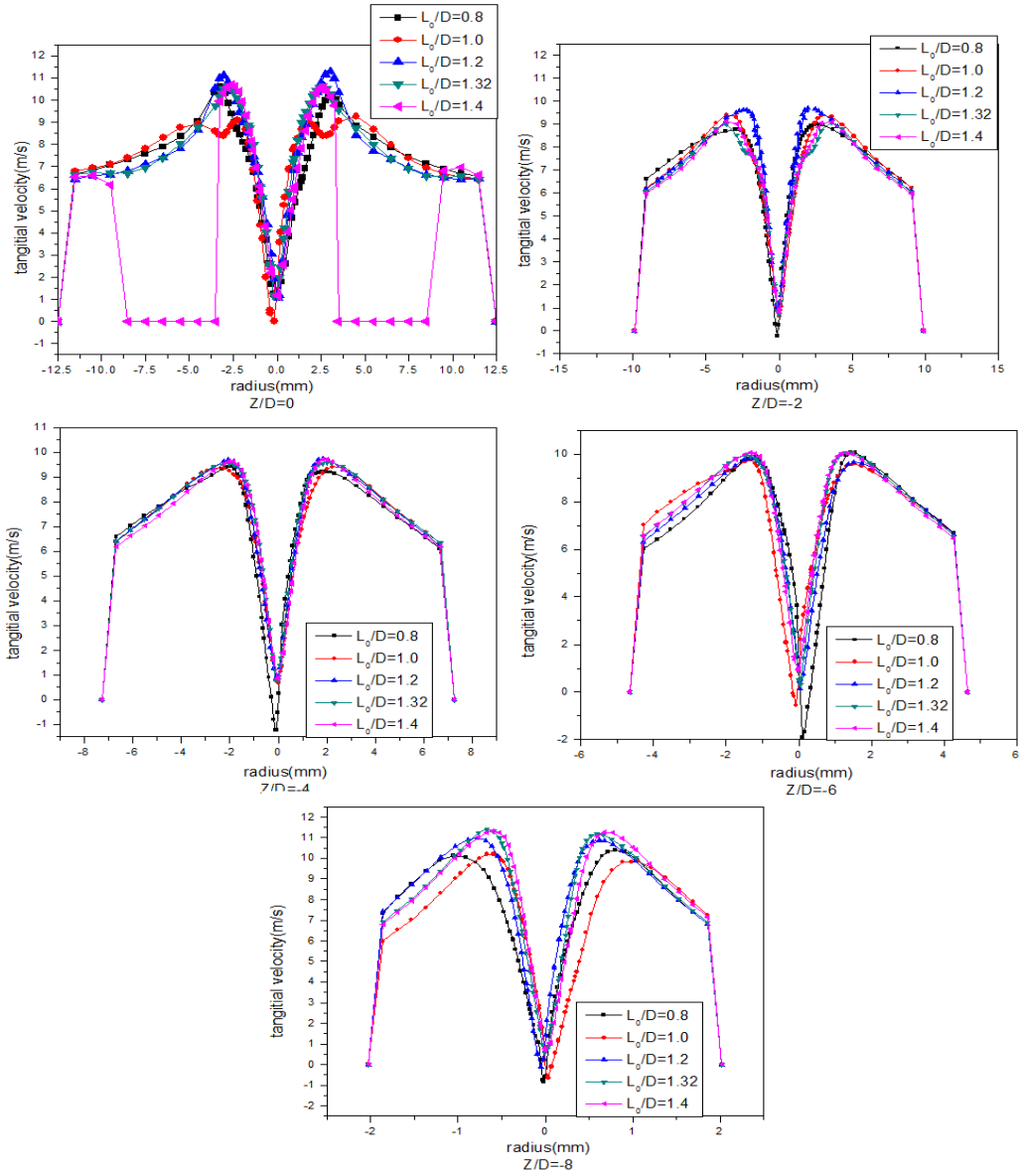

Figure 8. Tangential velocity comparative analysis chart of mini-hydrocycloness with different vortex finder depth.

4.1.4. Analysis of Streamline Diagram

It can be seen in Figure 9 that the secondary vortexes present spiral distribution on the periphery of the central axis when the vortex finder depth of mini-hydrocyclones is 0.8, 1.0, and 1.2. However, when the vortex finder depth reaches 1.32 or up, the structure of the vortex changes greatly, the secondary vortexes spiral distribution is moved down to the middle and lower cone of the mini-hydrocyclones. It is obvious that vortex finder depth has influence on flow field and the formation of the secondary vortex.

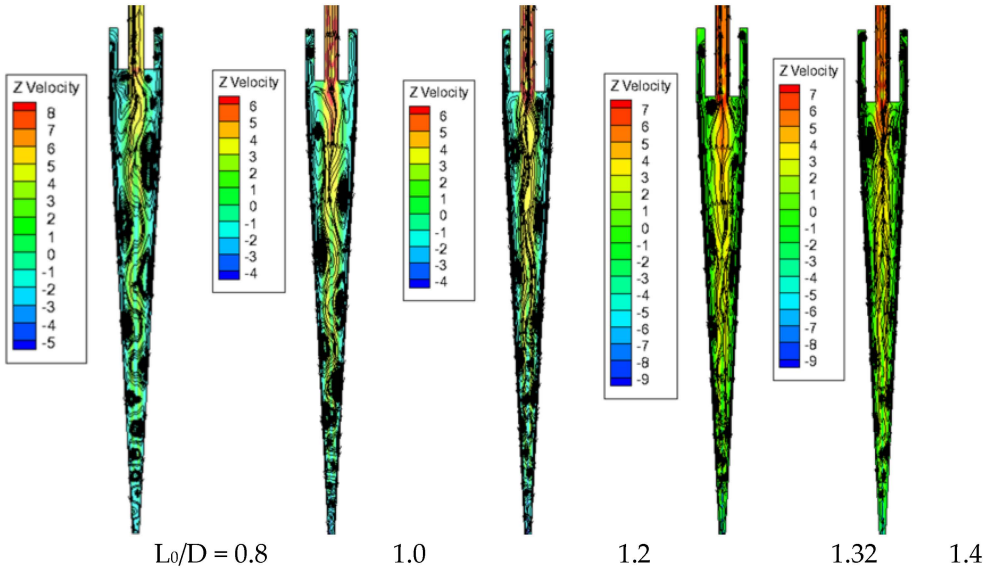

Figure 9. Streamline diagram of mini-hydrocycloness with different vortex finder depth.

4.1.5. Analysis on Locus of Zero Vertical Velocity (LZVV)

It demonstrates in Figure 10 that LZVV is not a cone. the bottom of the LZVV concave to a different degree. LZVV also is not an entire body, there are some small zones of LZVV near the underflow outlet and the vicinity of the ring gap between vortex finder and wall of mini-hydrocyclones. Particles may stay in LZVV of the ring gap for a long time and affect the separation efficiency. The LZVV near the underflow outlet is disconnected from the main body of LZVV. The particle in this area will eventually flow out from the underflow outlet except for a long stay. Concave in the main LZVV body reflects the back-mixing phenomenon. The underflow back-mixing is the most severe when the vortex finder L_0/D is 0.8, and situation is the best when the vortex finder L_0/D is 1.0.

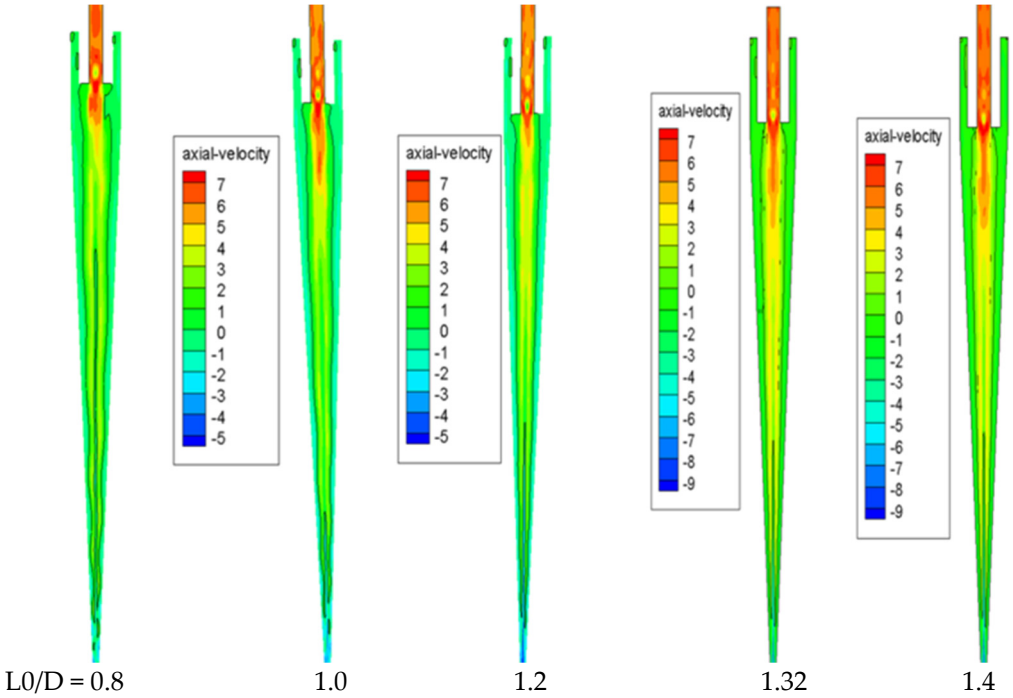

Figure 10. Figure 10 Locus of Zero Vertical Velocity of mini-hydrocycloness with different vortex finder depth.

4.1.6. Analysis of Turbulent Kinetic Energy Characteristics

Definition of the turbulent kinetic energy is shown in Equation (13), where $\overline{u}', \overline{v}', \overline{w}'$ are Root-Mean-Square (RMS) values of pulsating velocity in the three directions of x, y, and z-axis, respectively. The turbulent kinetic energy distribution is shown in Figure 11. It can be seen in each mini-hydrocyclones, the turbulent kinetic energy exhibits an axisymmetric distribution. Turbulent kinetic energy is relatively larger in the vicinity of vortex finder and underflow outlet than it is in the other region. The deeper the vortex finder inserts, the greater the turbulent kinetic energy near the vortex finder, accordingly, the bigger the energy consumption is.

$$K = \frac{\overline{u}' + \overline{v}' + \overline{w}'}{3} \tag{14}$$

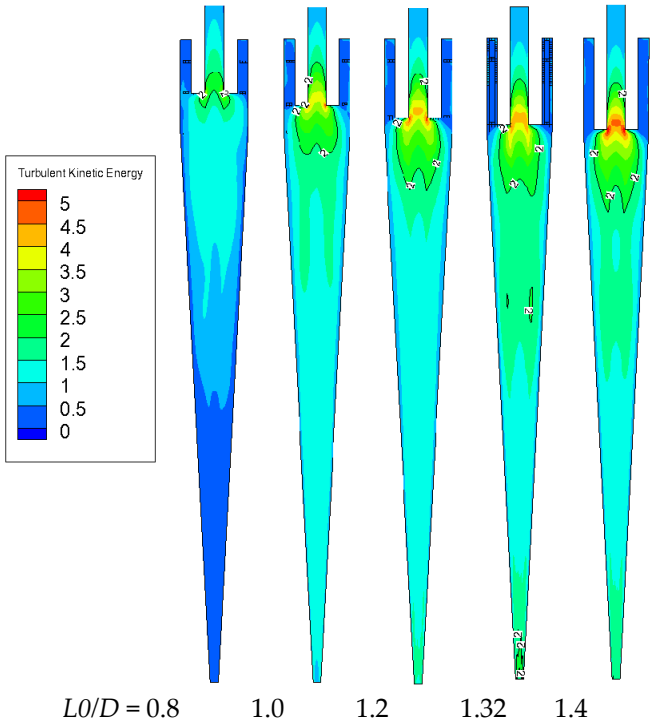

Figure 11. The turbulent kinetic energy of mini-hydrocycloness with different vortex finder depth.

4.2. Dispersed Phase

4.2.1. Separation Efficiency

Separation efficiency results of mini-hydrocycloness are shown in Figure 12. Separation experiment operation condition is 875 L/h, and the corresponding CFD simulation inlet velocity is 7.6 m/s. It can be seen that the agreement between simulation results and experiment is good, but separation efficiency of simulation is a little higher than that of experiment to every mini-hydrocycloness, because simulation process did not consider changes of environmental factor. It also demonstrates that the highest separation efficiency does not belong to the hydrocyclone which its vortex finder depth is the deepest or the shallowest. It indicated that L_0/D of the optimal vortex finder depth for hydrocyclone is around 1.0.

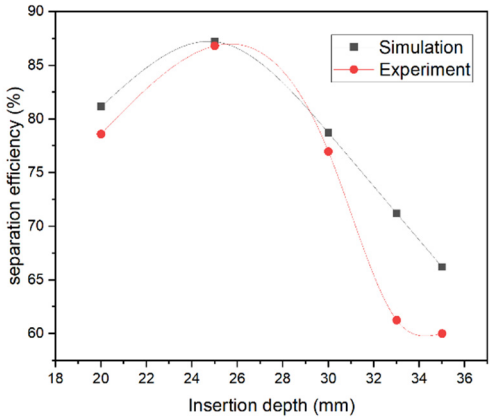

Figure 12. Separation efficiency of mini-hydrocycloness with different vortex finder depth.

4.2.2. Dispersed Phase Particle Concentration Distribution

Concentration of seven cross-sections of mini-hydrocycloness with different vortex finder depth is shown in Figure 13. It illustrates that the deeper the vortex finder inserts, the closer the area which still exist solid particles is to the central of hydrocylone, and the bigger the pre-separation zone volume. The main separation zone migrates to the underflow outlet direction. It is unfavourable to improve separation performance of mini-hyodrocyclone.

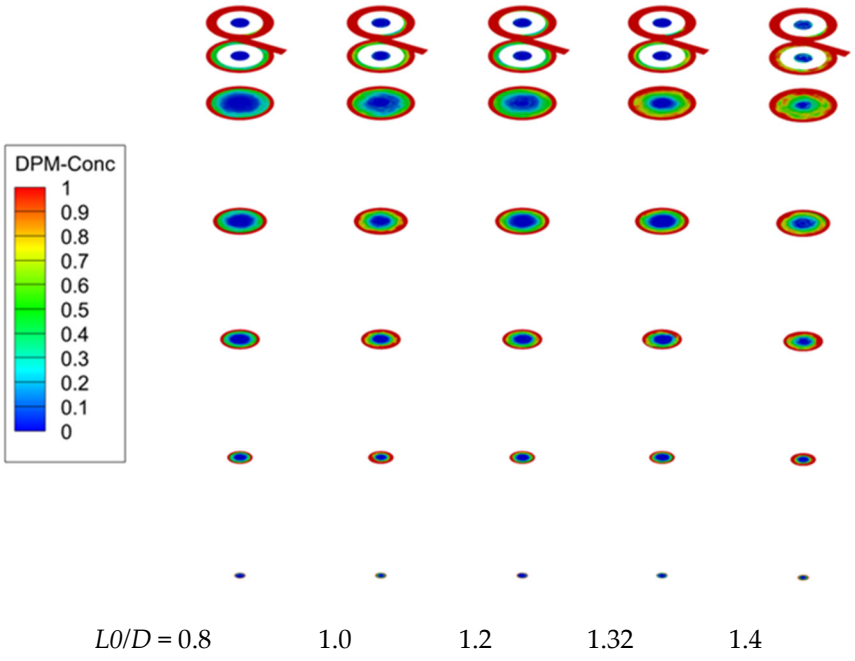

Figure 13. Concentration distribution of mini-hydrocycloness with different vortex finder depth.

5. Conclusions

The finding of this study can be summarized as follows: (1) Vortex finder has a significant influence on the functional partition of mini-hydrocyclones. The volume of the pre-separation zone gets larger with the deeper vortex finder depth, according, and the main separation zone is compressed. The phenomena of flow back-mixing are the most severe when vortex finder depth is 0.8, and the situation is best and the main separation zone is also the biggest when the depth is 1.0. Vortex finder depth also has a significant impact on the radial velocity in the main separation zone. The deeper the vortex finder depth, the smaller the radial velocity. (2) At the inlet of the vortex finder and the outlet of mini-hydrocyclones, the turbulent energy is bigger than the other region. The deeper the vortex finder depth inserts, the bigger the energy consumes. (3) The separation performance

of mini-hydrocyclone can be promoted by flow field structures of mini-hydrocycloness. The flow field is better to the separation process when L_0/D is 1.0. (4) L_0/D of the optimal vortex finder depth for hydrocyclone is around 1.0.

In future work, we plan to build a predictive model using a machine learning approach. We hope that through the predictive model, the optimal vortex finder depth can be obtained at a minimum cost.

Author Contributions: Conceptualization, F.H.; methodology, J.W. and Y.H.; software, F.H., D.Z. and Q.L.; validation, F.H. and D.Z.; formal analysis, F.H.; investigation, F.H., J.W. and Y.H.; resources, F.H.; data curation, F.H. and D.Z.; writing—original draft preparation, F.H. All authors have read and agreed to the published version of the manuscript.

Funding: F. He would like to acknowledge the sponsorship of the National Science Foundation of China (51608325, 52000071) for financial support.

Institutional Review Board Statement: The study didn't involve any studies on humans or animals.

Informed Consent Statement: Not applicable.

Data Availability Statement: The data presented in this study are available on request from the corresponding author.

Conflicts of Interest: No conflict of interest exists in the submission of this manuscript, and manuscript is approved by all authors for publication.

Nomenclature

Symbols

D	diameter of the cyclone separator's cylindrical section (mm)
L_0	vortex finder depth of the mini-hydrocyclones (mm)
L_S	cylindrical length of the mini-hydrocyclones (mm)
a	inlet width (mm)
b	inlet height (mm)
θ	cone angle (°)
d_u	underflow orifice diameter of the mini-hydrocyclones (mm)
d_0	overflow orifice diameter of the mini-hydrocyclones (mm)
C	constant
u	Velocity of continuous phase (mm)
P	pressure (Pa)
ρ	particle density (kg/m3)
I	turbulence intensity
k	turbulent kinetic energy
ε	turbulent dissipation rate
$\overline{u}$	time-average pulsation velocity of the turbulent flow
l	turbulent feature size
D_H	hydraulic diameter
C_μ	empirical constant
Re	Reynolds number
u_{in}	inlet velocity (m/s)
R	Radial location (mm)
$\overline{u}'$	RMS values of pulsating velocity of x
$\overline{v}'$	RMS values of pulsating velocity of y
$\overline{w}'$	RMS values of pulsating velocity of z
η	separation efficiency
m_u	the mass flow rate of dispersed phase solid particles at the underflow outlet
m	the mass flow rate of dispersed phase solid particles at the inlet

References

1. Liu, Y.; Lu, H.; Li, Y.; Xu, H.; Pan, Z.; Dai, P.; Wang, H.; Yang, Q. A review of treatment technologies for produced water in offshore oil and gas fields. *Sci. Total Environ.* **2021**, *775*, 145485. [CrossRef] [PubMed]
2. Liu, Y.; Lu, H.; Liu, P.; Li, Y.; Wu, S.; Dai, P.; Yang, Q. Treatment of the complex liquid phase that contains produced water, condensate oil, and floccule from an offshore gas field: A pilot system for the South China Sea. *J. Nat. Gas Sci. Eng.* **2021**, *94*, 104125. [CrossRef]
3. Guo, J.; Gong, D.-T.; Zhang, J.; Wang, L.-Y.; Zheng, Z.-C.; Li, K.-M. Studies on mechanism of sand removal from crude oil. *J. Hydrodyn.* **2006**, *18*, 385–390. [CrossRef]
4. Mohanty, S.; Das, B. Optimization studies of hydrocyclone for beneficiation of iron ore slimes. *Miner. Process. Extr. Metall. Rev.* **2010**, *31*, 86–96. [CrossRef]
5. Xu, P.; Wu, Z.; Mujumdar, A.; Yu, B. Innovative hydrocyclone inlet designs to reduce erosion-induced wear in mineral de-watering processes. *Dry. Technol.* **2009**, *27*, 201–211. [CrossRef]
6. Liu, Y.; Wang, H.-L.; Xu, Y.-X.; Fang, Y.-Y.; Chen, X.-R. Sludge disintegration using a hydrocyclone to improve biological nutrient removal and reduce excess sludge. *Sep. Purif. Technol.* **2017**, *177*, 192–199. [CrossRef]
7. Pan, G.; Chang, Y.; Fu, M. Computational fluid dynamics analysis of shroud design on hemodynamic performance and blood damage in a centrifugal blood pump. *Comput. Model. Eng. Sci.* **2018**, *116*, 199–213. [CrossRef]
8. Bai, Z.S.; Wang, H.L.; Tu, S.T. Numerical and experimental study on the removal of catalyst particles from oil slurry by hydrocyclone. *Pet. Sci. Technol.* **2010**, *28*, 525–533. [CrossRef]
9. Yang, Q.; Li, Z.-M.; Lv, W.-J.; Wang, H.-L. On the laboratory and field studies of removing fine particles suspended in wastewater using mini-hydrocyclones. *Sep. Purif. Technol.* **2013**, *110*, 93–100. [CrossRef]
10. He, L.; Ji, L.; He, Y.; Liu, Y.; Chen, S.; Chu, K.; Kuang, S. Experimental and numerical analysis of Chinese hamster ovary cell viability loss in mini-hydrocycloness. *Sep. Purif. Technol.* **2022**, *295*, 121203. [CrossRef]
11. Raesi, R.; Maddahian, R. Numerical investigation of air-injected deoiling hydrocyclones using population balance model. *Chem. Eng. Sci.* **2022**, *248*, 117103. [CrossRef]
12. He, F.; Wang, H.; Wang, J.; Li, S.; Fan, Y.; Xu, X. Experimental study of mini-hydrocyclones with different vortex finder depths using Particle Imaging Velocimetry. *Sep. Purif. Technol.* **2020**, *236*, 116296. [CrossRef]
13. He, F.; Zhang, Y.; Wang, J.; Yang, Q.; Wang, H.; Tan, Y. Flow Patterns in Mini-hydrocycloness with Different Vortex Finder Depths. *Chem. Eng. Technol.* **2013**, *36*, 1935–1942. [CrossRef]
14. Bhattacharyya, P. Theoretical study of the flow field inside a hydrocyclone with vortex finder diameter greater than that of apex opening—II. Turbulent case. *Appl. Sci. Res.* **1980**, *36*, 213–225. [CrossRef]
15. Liu, Y.; Yang, Q.; Qian, P.; Wang, H.-L. Experimental study of circulation flow in a light dispersion hydrocyclone. *Sep. Purif. Technol.* **2014**, *137*, 66–73. [CrossRef]
16. Wang, B.; Yu, A. Numerical study of the gas–liquid–solid flow in hydrocyclones with different configuration of vortex finder. *Chem. Eng. J.* **2008**, *135*, 33–42. [CrossRef]
17. Lv, W.J.; Huang, C.; Chen, J.Q.; Liu, H.L.; Wang, H.L. An experimental study of flow distribution and separation performance in a UU-type mini-hydrocyclones group. *Sep. Purif. Technol.* **2015**, *150*, 37–43. [CrossRef]
18. Zhao, Q.; Cui, B.; Wei, D.; Song, T.; Feng, Y. Numerical analysis of the flow field and separation performance in hydrocyclones with different vortex finder wall thickness. *Powder Technol.* **2019**, *345*, 478–491. [CrossRef]
19. Oliveira, D.; Almeida, C.; Vieira, L.; Damasceno, J.; Barrozo, M. Influence of geometric dimensions on the performance of a filtering hydrocyclone: An experimental and CFD study. *Braz. J. Chem. Eng.* **2009**, *26*, 575–582. [CrossRef]
20. Vega-Garcia, D.; Brito-Parada, P.; Cilliers, J. Optimising small hydrocyclone design using 3D printing and CFD simulations. *Chem. Eng. J.* **2018**, *350*, 653–659. [CrossRef]
21. Li, F.; Liu, P.; Yang, X.; Zhang, Y.; Li, X.; Jiang, L.; Wang, H.; Fu, W. Numerical Analysis on the Effect of Combined-Curve Tapered Segment on the Flow Field and Separation Performance of Hydrocyclones. *Arab. J. Sci. Eng.* **2022**, *47*, 6193–6207. [CrossRef]
22. Niazi, S.; Habibian, M.; Rahimi, M. Performance evaluation of a uniflow mini-hydrocyclones for removing fine heavy metal particles from water. *Chem. Eng. Res. Des.* **2017**, *126*, 89–96. [CrossRef]
23. Yang, Q.; Lv, W.-J.; Ma, L.; Wang, H.-L. CFD study on separation enhancement of mini-hydrocyclones by particulate arrangement. *Sep. Purif. Technol.* **2013**, *102*, 15–25. [CrossRef]
24. Vakamalla, T.R.; Koruprolu, V.B.R.; Arugonda, R.; Mangadoddy, N. Development of novel hydrocyclone designs for improved fines classification using multiphase CFD model. *Sep. Purif. Technol.* **2017**, *175*, 481–497. [CrossRef]
25. Xu, J.R.; Luo, Q.; Qiu, J.C. Research on the preseparation space in hydrocyclones. *Int. J. Miner. Process.* **1991**, *31*, 1–10. [CrossRef]
26. Wang, C.C.; Wu, R.M. Experimental and simulation of a novel hydrocyclone-tubular membrane as overflow pipe. *Sep. Purif. Technol.* **2018**, *198*, 60–67. [CrossRef]
27. Olson, T.; Van Ommen, R. Optimizing hydrocyclone design using advanced CFD model. *Miner. Eng.* **2004**, *17*, 713–720. [CrossRef]
28. Ni, L.; Tian, J.; Song, T.; Jong, Y.; Zhao, J. Optimizing geometric parameters in hydrocyclones for enhanced separations: A review and perspective. *Sep. Purif. Rev.* **2019**, *48*, 30–51. [CrossRef]
29. Slack, M.; Del Porte, S.; Engelman, M. Designing automated computational fluid dynamics modelling tools for hydrocyclone design. *Miner. Eng.* **2004**, *17*, 705–711. [CrossRef]
30. Murthy, Y.R.; Bhaskar, K.U. Parametric CFD studies on hydrocyclone. *Powder Technol.* **2012**, *230*, 36–47. [CrossRef]

31. Jing, J.; Zhang, S.; Qin, M.; Luo, J.; Shan, Y.; Cheng, Y.; Tan, J. Numerical simulation study of offshore heavy oil desanding by hydrocyclones. *Sep. Purif. Technol.* **2021**, *258*, 118051. [CrossRef]
32. Zhao, Z.; Zhou, L.; Liu, B.; Cao, W. Computational fluid dynamics and experimental investigation of inlet flow rate effects on separation performance of desanding hydrocyclone. *Powder Technol.* **2022**, *402*, 117363. [CrossRef]
33. Wang, B.; Chu, K.; Yu, A.; Vince, A. Modeling the multiphase flow in a dense medium cyclone. *Ind. Eng. Chem. Res.* **2009**, *48*, 3628–3639. [CrossRef]
34. Pendar, M.R.; Esmaeilifar, E.; Roohi, E. LES study of unsteady cavitation characteristics of a 3-D hydrofoil with wavy leading edge. *Int. J. Multiph. Flow* **2020**, *132*, 103415. [CrossRef]
35. Pendar, M.R.; Roohi, E. Cavitation characteristics around a sphere: An LES investigation. *Int. J. Multiph. Flow* **2018**, *98*, 1–23. [CrossRef]